Additive-Free Hollow-Structured Co_3O_4 Nanoparticle Li-Ion Battery: The Origins of Irreversible Capacity Loss

Youngjun Kim,[†,+] Jung-Hyun Lee,[‡,+] Sungeun Cho,[†] Yongwoo Kwon,[†] Insik In,[§] Jihoon Lee,[§] Nam-Ho You,[⊥] Elsa Reichmanis,[∥] Hyungduk Ko,[#] Kyu-Tae Lee,[#,¶] Hyun-Keun Kwon,[#,¶] Doo-Hyun Ko,[#,*] Heesun Yang,[†,*] and Byoungnam Park[†,*]

[†]Department of Materials Science and Engineering, Hongik University 72-1, Sangsu-dong, Mapo-gu, Seoul 121-791, Korea, [‡]Department of Chemical and Biological Engineering, Korea University, Anam-dong, Sungbuk-gu, Seoul 136-713, Korea, [§]Department of Polymer Science and Engineering & Department of IT Convergence, Korea National University of Transportation, Chungju 380-702, Korea, [⊥]Carbon Convergence Materials Research Center, Institute of Advanced Composites Materials, Korea Institute of Science and Technology, Jeollabuk-do 565—905, Korea, [∥]School of Chemical and Biomolecular Engineering, Georgia Institute of Technology, Atlanta, Georgia 30332, United States, [#]Center for Optoelectronic Convergence Systems, Korea Institute of Science and Technology, Seoul 136-791, Korea, and [¶]Display and Nanosystem Laboratory, College of Engineering, Korea University, Seoul 136-713, Korea. [+]Youngjun Kim and Jung-Hyun Lee contributed equally to the paper.

ABSTRACT Origins of the irreversible capacity loss were addressed through probing changes in the electronic and structural properties of hollow-structured Co_3O_4 nanoparticles (NPs) during lithiation and delithiation using electrochemical Co_3O_4 transistor devices that function as a Co_3O_4 Li-ion battery. Additive-free Co_3O_4 NPs were assembled into a Li-ion battery, allowing us to isolate and explore the effects of the Co and Li_2O formation/decomposition conversion reactions on the electrical and structural degradation within Co_3O_4 NP films. NP films ranging between a single monolayer and multilayered film hundreds of nanometers thick prepared with blade-coating and electrophoretic deposition methods, respectively, were embedded in the transistor devices for *in situ* conduction measurements as a function of battery cycles. During battery operation, the electronic and structural properties of Co_3O_4 NP films in the bulk, Co_3O_4/electrolyte, and Co_3O_4/current collector interfaces were spatially mapped to address the origin of the initial irreversible capacity loss from the first lithiation process. Further, change in carrier injection/extraction between the current collector and the Co_3O_4 NPs was explored using a modified electrochemical transistor device with multiple voltage probes along the electrical channel.

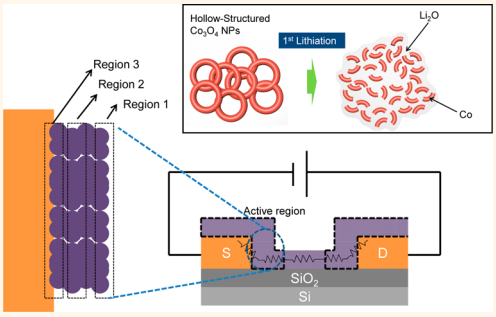

KEYWORDS: cobalt oxide · conversion reaction · capacity loss · Li-ion battery · nanoparticle

Nanostructured materials are emerging as attractive electrode materials for use in Li-ion batteries because they exhibit better adaptability to the strain arising from Li insertion/removal, thereby improving electrochemical cyclability.[1−4] Shorter path lengths for electronic and ionic transport can be achieved with nanosized building blocks facilitating reversible electrochemical reactions.[5−8] Further, the large surface area of nanomaterials allows for high charging/discharging rates because of increased Li-ion flux through the liquid electrolyte/nanosized electrode material interface.

Particularly, nanostructured transition metal oxide anode materials have been a focal point due to their high specific capacity and excellent cycle reversibility.[9−11] The relatively low gravimetric capacity of less than 370 mAh/g of carbon has motivated their development. Poizot *et al.* demonstrated nanosized transition metal oxides as anodes and explored their high capacity and cyclability during lithiation and delithiation.[11] Importantly, it was proposed that the reaction mechanism associated with transition metal oxides is distinctly different from the classical mechanism where charging/discharging occurs through intercalation and deintercalation of Li into the electrode material. In the case of CoO, an abrupt structural change was observed during battery charging/discharging cycles, with the formation of metallic Co and conversion of Li to Li_2O phases.[12] Recently, Ha *et al.* reported fabrication of a Co_3O_4 nanoparticle Li-ion battery without the use of additives such as

* Address correspondence to metalpbn@hongik.ac.kr, dhko@kist.re.kr, hyang@hongik.ac.kr.

Received for review January 13, 2014 and accepted June 4, 2014.

Published online June 04, 2014
10.1021/nn500218m

conductive agents and polymer binders.[13] A high specific capacity close to the theoretical capacity (~890 mAh/g) for Co_3O_4 NPs was obtained, and excellent cyclability was observed.

Despite the excellent specific capacity, an initial capacity loss continues to be observed reproducibly for transition metal oxides.[14] The formation of a passivation layer on the surface of electrode material and (or) incomplete decomposition of Li_2O in the conversion reaction have been suspected as possible origins of the initial large irreversible loss.[15,16] Battery charging/discharging processes involve a series of reactions in the bulk and at interfaces including charge transfer at the electrode/electrolyte interface,[17−20] diffusion of Li ions in the bulk,[20] and charge transfer/transport of electronic carriers.[10,18,21] Thus, the origin of the irreversible capacity loss needs to be explored in the context of whole battery operation. With the use of nanosized materials as electrode materials, electrochemical reactions at the electrode/electrolyte and the electrode/current collector interfaces become signficantly more important because of the increased surface area *versus* that for microsized alternatives. For nanostructured materials then, the contribution of the interfacial reactions in determining specific capacity and cyclability is significant. Therefore, a comprehensive study examining the nanostructured materials' interfaces, including NP/electrolyte, NP/NP in the bulk, and the current collector/NP interfaces, is essential to understand the relevant electrochemical and (or) electronic reactions associated with the observed initial capacity loss.

In carrying out a comprehensive study of the origins of irreversible capacity loss, a challenge is the use of additives such as conductive agents and polymer binders. In integrating nanostructured materials into Li-ion batteries, the use of additives has complicated analysis of the physical and electrochemical reactions that occur between Li ions and the nanostructured materials. Particularly, the large surface area of nanostructured electrodes can be detrimental because the formation of heterojunction interfaces involving additives can induce carrier trapping centers and hamper reversible electrochemical reactions.[22] Therefore, to probe the inherent electrode material's electronic and structural properties during lithiation and delithiation, without being distracted by complications arising from additives, a "good" Li-ion battery structured solely with nanostructured materials is required.

In this paper, we explore the origins of the irreversible capacity loss by probing changes in the electronic and structural properties of hollow-structured Co_3O_4 nanoparticles (NPs) that arise during lithiation and delithiation. Additive-free Co_3O_4 NPs were incorporated into the channel in a two-contact transistor device in which source and drain electrodes serve as current collectors. This arrangement allows for isolating and exploring the buried Co_3O_4 bulk, Co_3O_4 NPs/electrolyte, and Co_3O_4 NPs/current collector interfaces during the Co and Li_2O formation/decomposition conversion reactions. Structural changes in Co_3O_4 NP films, prepared using blade-coating and electrophoretic deposition (EPD) methods, ranging in thickness from a single monolayer to tens of layers within the first few cycles were correlated with the change in electronic charge transport properties using a modified electrochemical transistor device. Co_3O_4 NPs in the electrical channel of the transistor device were "structurally doped" with the formation of Co and lithia (Li_2O) *via* Li insertion into the electrical channel. Using two-contact and multiple voltage probe devices in combination with electrostatic force microscopy (EFM) and atomic force microscopy (AFM), electronic charge transport within NP films and electronic charge injection/extraction properties through the current collector/Co_3O_4 NP interface were explored and coupled to the initial irreversible capacity loss.

RESULTS

Co_3O_4 NPs were assembled into monolayer scale and thick films using blade-coating (see the Supporting Information Figure S1) and EPD methods, respectively, in Figure 1a. The electrochemical apparatus to control Li insertion and deinsertion for Co_3O_4 NPs embedded in a two-contact electrochemical transistor device is shown in Figure 1b. To monitor the change in the electronic conduction during the battery cycles, we designed a modified electrochemical two-contact transistor device in which a Co_3O_4 NP film is deposited between the Pt source and drain electrodes patterned photolithographically onto a SiO_2 substrate (Figure 1c). In the device, the whole area except the Co_3O_4 film between the metal electrodes is covered by epoxy to prevent electrochemical reactions with liquid electrolyte (1 M $LiClO_4$) as seen in Figure 1c. Co_3O_4 NPs between the metal electrodes (*i.e.*, current collectors) are in direct contact with liquid electrolyte to participate in the battery charging/discharging processes. As a reference/counter electrode, a Li metal flake was used. The source and drain electrodes were sustained at the same potential during lithiation (discharging) and delithiation (charging) processes. Transistor devices with a channel length between 20 and 50 μm were used. After charging/discharging processes in a liquid electrolyte (Figure 1b), the two-contact device was rinsed with dimethyl carbonate (DMC) several times and dried in a glovebox to eliminate remnant $LiClO_4$ and solvent on the surface of the Co_3O_4 film that may modify electronic conduction. For electrical characterization using the structure in Figure 1c, a small source−drain voltage ranging between −1 and 1 V was applied to measure the change in the electronic conduction in the Co_3O_4 NP film as a result of lithiation and delithiation. Co_3O_4 NP films in the device were

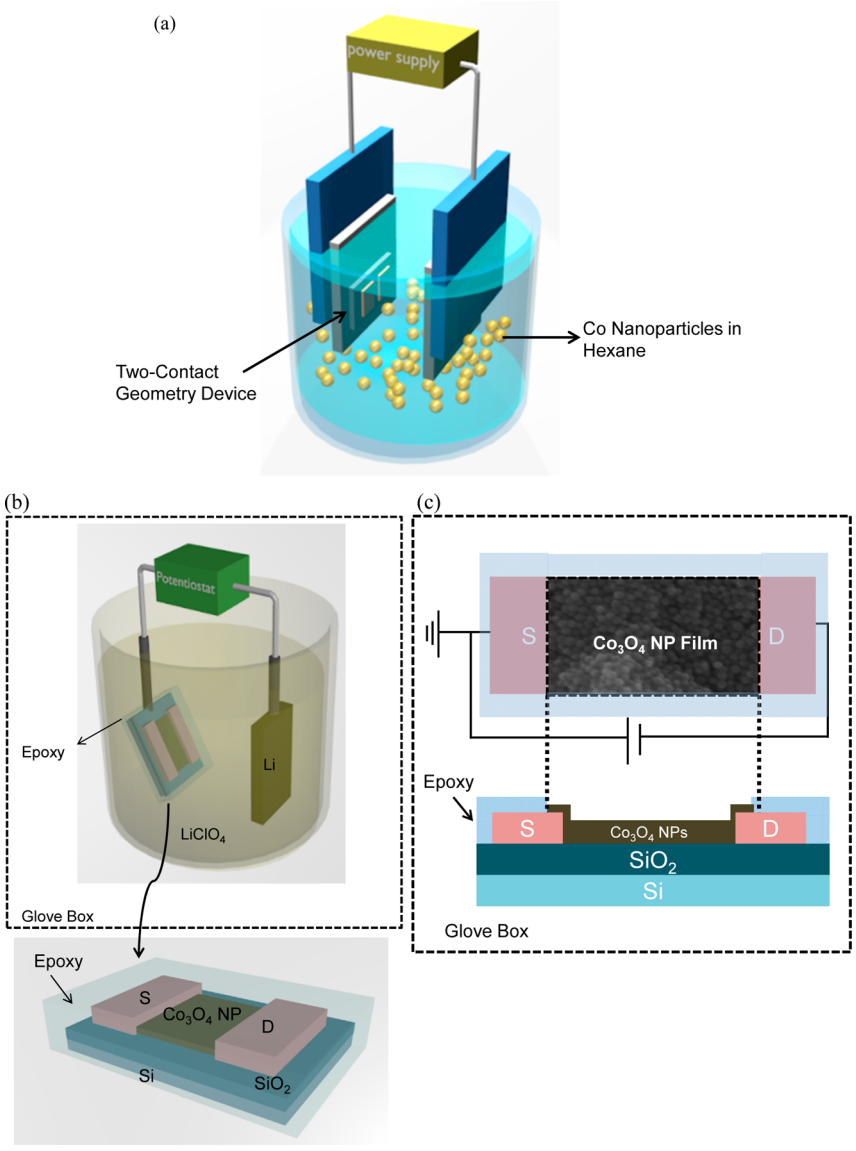

Figure 1. Schematic diagrams of the setup for (a) depositing a Co_3O_4 NP film using the electrophoretic deposition method and (b) lithiation and delithiation of Co_3O_4 NP films embedded in a two-contact geometry device. (c) Schematic diagram of the two contact geometry transistor device. The device is covered with epoxy except the Co_3O_4 NP channel region.

charged and discharged between 3.0 and 0.05 V, respectively. All electrical and battery characterizations (charging and discharging) were performed in an Ar-filled glovebox. EFM and AFM were used to investigate the change in surface potential of Co_3O_4 NP films with morphological evolution depending on electrochemical reactions.

Irreversible Capacity Loss in Co_3O_4 NPs. Electrochemical reactions of a Co_3O_4 NP thick and monolayer films with Li ions are demonstrated *via* battery charging/discharging curves in Figure 2. Oxidation and reduction reactions of Co_3O_4 NPs are characterized by cyclic voltametry (CV) (see Supporting Information Figure S2). Reduction peaks at 0.70 and 1.35 V and oxidation peaks at 2.20 V were observed and are consistent with those from previous studies.[23,24] Particularly, the peak at 0.70 V was attributed to the formation of Li_2O as well as solid electrolyte interphase (SEI) layer. Thicker Co_3O_4 NP films (~400 nm) are shown in Figure 2a. In the plot of potential *versus* specific capacity, a high capacity of ~1300 mAh/g in the first discharge was observed at a current density of 100 mAg^{-1} between 0.1 and 3.0 V, a value which is higher than that estimated from theoretical calculations (~890 mAh/g). In the first discharge curve, a longer sloping region was observed with a higher capacity than the theoretical capacity. Particularly, the discharge slope appeared approximately at 0.7 V, corresponding to the formation of the SEI layer. The stabilized specific capacity of about 800 mAh/g was observed after three cycles which exhibited a large initial Coulombic loss consistent with previous studies.[13] For the three discharge curves, the potentials dropped rapidly up to ~1.6 V followed by the first sloping region between 1.6 and 0.8 V, consistent with

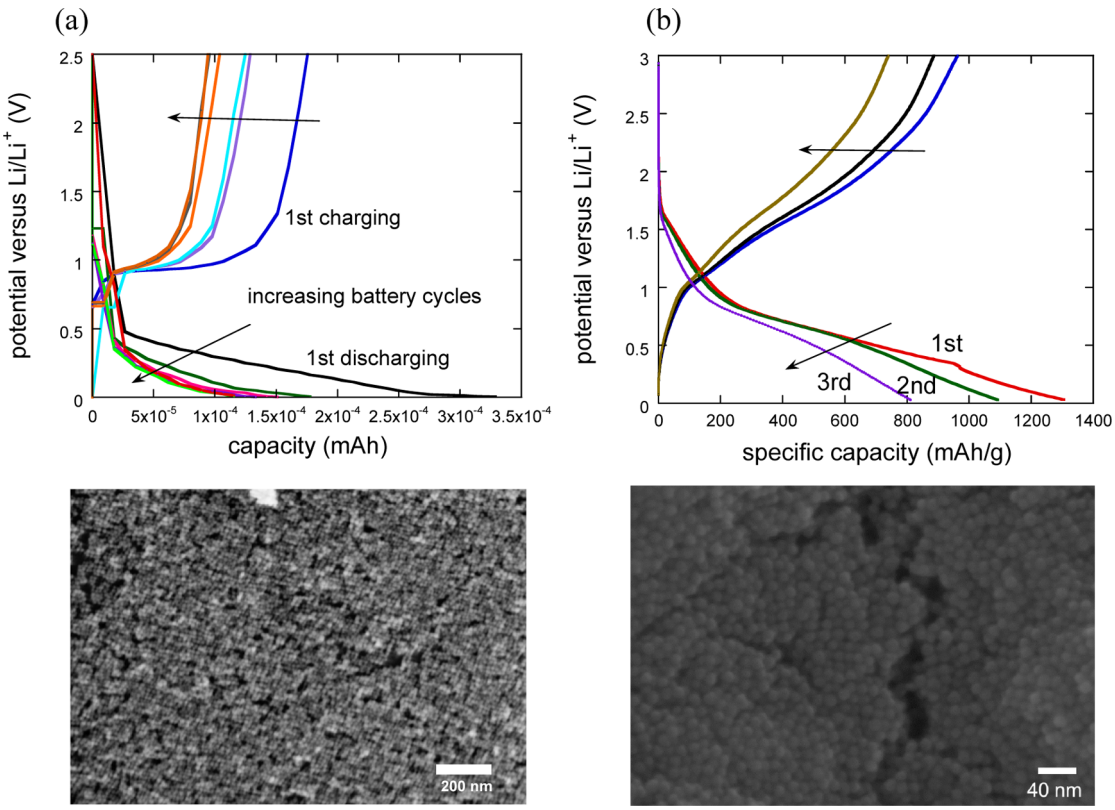

Figure 2. Initial charge–discharge curves and scanning electron microscopy images for (a) Co_3O_4 monolayer and (b) thick films.

the reduction peak at 1.4 V in the CV curve arising from lithiation of Co_3O_4 electrode. During the delithation process (charging), a sloping region between 1.7 and 2.2 V matches well with the oxidation peak at 2.19 V in the CV measurement.

Charging/discharging curves and a scanning electron microscopy (SEM) image of a monolayer thick Co_3O_4 NP film deposited onto a SiO_2 substrate are shown in Figure 2b. The film does not completely cover the SiO_2 substrate as can be seen from the dark colored regions (SiO_2 substrate) between Co_3O_4 NPs. Clearly, however, the NPs have formed a percolation network on the substrate, forming lateral current paths as confirmed by current–voltage measurements (Figure S3a). The initial Coulombic efficiency was only 55%, far lower than 85% obtained with the multilayered thicker film shown in Figure 2a. The specific capacity for the monolayer thick sample could not be estimated due to the low number of Co_3O_4 NPs deposited in a small area of 5×10^{-4} cm^2 which corresponds to the channel area between the metal electrodes. Importantly, the high (greater than 800 mAh/g) specific capacity found for thick Co_3O_4 films embedded in a two-contact transistor device provides suppportive evidence that a large fraction of the electrical channel in the device participated in the charging/discharging processes. The region in which Li ions diffuse and contribute to the capacity is referred to as the "active region".

Conversion Reaction in Large Area. Probing change in the electronic charge transport in Co_3O_4 NP films as a result of charging/discharging processes can offer insights into the electronic and structural changes that occur over a large area of Co_3O_4 NPs buried in the film. Figure 3a depicts a device structure used for the electronic transport measurements in which the electronic conductance is monitored as a function of Li composition in Co_3O_4 NP films. The interdigitated Pt fingers are spaced by 20 μm, and the width of the channel was 5 mm. To lithiate and delithiate Co_3O_4 NPs, the source and drain electrodes were maintained at the same potential by wiring them together. In other words, the source and drain electrodes serve as a current collector at the same potential, and the Co_3O_4 NPs between the electrodes are the electrochemically active region through which Li ions diffuse.

Intrinsic electrical properties of Co_3O_4 NPs, before electrochemical reactions, were investigated using temperature-dependent current–voltage measurements. In the current *versus* voltage plot shown in Figure 3b, the electrical conductance increased with increasing temperature, indicating that carrier hopping through localized states in Co_3O_4 NP films governs electronic conduction in the channel. In the transport mechanism, carriers transport through the film by repeated "trapping in and releasing from" localized states located in the energy band tail.[25] Therefore, fewer trap sites enhance carrier mobility by increasing the mean free

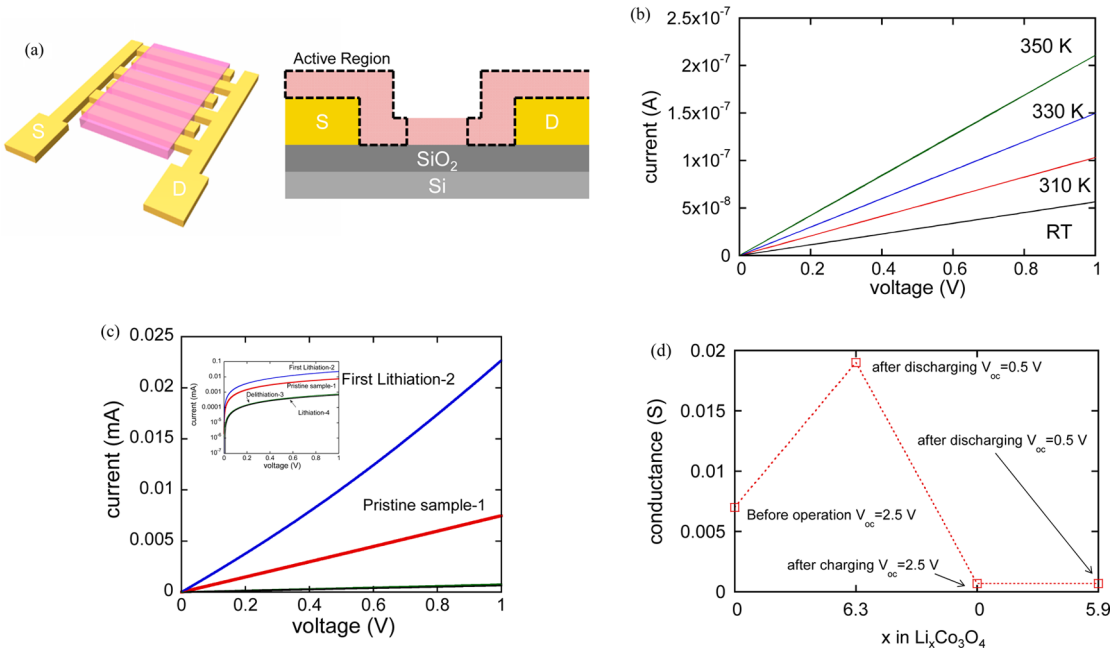

Figure 3. Electronic conduction measurement during charging/discharging processes. (a) Schematic diagram of a two-contact device with interdigitated fingers with a spacing of 20 μm. Co_3O_4 NPs are deposited using EPD. The active region in which Li ions diffuse is approximated with the dashed line. (b) Temperature-dependent *I*−*V* curves for a thick Co_3O_4 NP film. (c) *I*−*V* curves during lithiation and delithiation of a Co_3O_4 NP film. (d) Plot of conductance as a function of the Li composition change in Co_3O_4 NP film. The conductance value was obtained from *I*−*V* measurements in (c).

path of carriers.[25,26] From the temperature-dependent measurements, an activation energy of 130 meV for thermal-assisted hopping transport was calculated from the Arrhenius equation. This value was smaller than 280 meV from a monolayer thick Co_3O_4 film (Supporting Information Figure S3a). Indeed, the hole mobilities of the Co_3O_4 films were 1.5×10^{-5} and 3.7×10^{-9} cm^2/Vs, for thick and monolayer films, respectively, assuming a Co_3O_4 carrier concentration of 3×10^{19} cm^{-3}.[28] This result indicates that the connectivity between NPs in the thicker film is far better in comparison to the monolayer structure.

Change in the electronic conductance of the thicker Co_3O_4 film was monitored after the film was lithiated up to V_{oc} = 0.05 V. In the current−voltage measurements shown in Figure 3c, the source−drain current increased by about a factor of 3 in the first discharge (First lithiation-2) in Figure 3c. After delithiation up to V_{oc} = 2.5 V ($Li_xCo_3O_4$), the current significantly decreased and was smaller than that for a pristine sample (Pristine sample-1). In the inset in Figure 3c, the current change was plotted on a logarithmic scale for clarification. Interestingly, the current further decreased in the following lithiation (Lithiation-4 in the inset in Figure 3c). The change in conductance as a result of the electrochemical reactions in Figure 3c is summarized in the plot of conductance as a function of Li composition in a Co_3O_4 film in Figure 3d.

This significant conductance change in the Co_3O_4 NP film results from structural changes coupled with variations of the chemical composition. Significant structural change after lithiation was observed in an earlier *ex situ* transmission electron microscopy (TEM) study.[13] It was observed that the polycrystalline hollow Co_3O_4 NPs do not retain their original shape after lithiation in the first cycle.[13] The Co_3O_4 NPs were found to break into smaller and less defined pieces based on TEM images. On the other hand, the conductance change arises from changes in the electronic properties of Co_3O_4 NPs associated with the change in the chemical composition caused by the conversion reaction.

The abrupt increase in the current after the first lithiation in Figure 3c is attributed to the formation of Co and Li_2O during the conversion reaction of Co_3O_4 as shown in the given equations.

$$Co_3O_4 + 8Li^+ + 8e^- \leftrightarrow 4Li_2O + 3Co^0$$
$$8Li \leftrightarrow 8Li^+ + 8e^-$$
$$Co_3O_4 + 8Li \leftrightarrow 4Li_2O + 3Co^0$$

Unlike classical Li alloying and dealloying processes, the conversion reaction produces a Co phase in a Li_2O matrix as a result of lithiation.[11] We suggest that, in the first discharge (First Lithiation-2 in Figure 3c), the significant conductance increase is due to the formation of a metallic Co phase accompanied by reduction of Co^{3+} and Co^{2+} forming Co^0, as evidenced by the two cathodic peaks as shown in Figure S2. Oxidation of Co and decomposition of Li_2O were inferred from the two oxidation peaks at 2.19 and 2.32 V in the following delithiation.[24] The conductance decrease during delithiation (Delithiation-3 in the inset in Figure 3c) can be attributed to the remnant Li_2O, hampering a reversible

electrochemical reaction into Co_3O_4 and Li. The electrically resistive Li_2O phase in the channel can destroy the efficient electronic conduction path. It is important to note that the peak at 0.70 V during the first discharge can be associated with fromation of the SEI layer on the surface of Co_3O_4.[14]

Interestingly, the current did not recover to its original value after subsequent lithiation (Lithiation-4 in the inset in Figure 3c) and remained constant at a lower value than that of the pristine. This observation suggests that the conduction path is disrupted in the first delithiation (charging) process and that the associated morphology change is not reversible, hampering efficient electronic transport. The details will be discussed later. Additionally, it was confirmed that the effect of remnant solvent in the Co_3O_4 NP film (DMC and ethylene carbonate (EC)) on electronic charge transport, if any, is negligible. We compared $I-V$ curves for two samples. One is a control sample without any electrochemical treatment. The other sample was dipped in DMC and EC solvent for 5−6 h and rinsed to remove any solvent adsorbed on the Co_3O_4 surface. The current−voltage curves for the two samples were similar.

It may be argued that the conductance increase after the first lithiaion in Figure 3d is far smaller than the prediction based on a metallic transition from Co_3O_4 to Co because a significant increase in carrier concentration and mobility is expected. Indeed, a hole mobility of Co_3O_4, 1.5×10^{-5} cm^2/Vs, estimated from a carrier concentration of 3×10^{19} cm^{-3} is far lower than Co by tens of orders of magnitude.[25] However, the structural arrangement with the formation of Li_2O can explain the very small conductance increase. It has been known that a metallic Co phase agglomerates and is dispersed in a Li_2O matrix,[12,16,27] failing to form an efficient charge transport path. This process leads to a significant decrease in the carrier mobility in the Co_3O_4 NP channel between the source and drain electrodes due to creation of an electrically resistive phase (*i.e.*, Li_2O), which hampers a dramatic current increase. In other words, the formation of Li_2O, a resistor with high impedance, should be considered to account for only a small current increase after lithiation.

After lithiation, the volume ratio calculated from the reaction between Co and Li_2O is about 1:3 assuming that Co and Li_2O phases are created at a ratio of 4:3. For a binary distribution of spheres with equisized particles, the 3D percolation threshold in the system is approximately 0.3 in volume fraction.[28] This indicates that at least the mixture of Co and Li_2O occupies 30% of the total volume in the electrical channel since the electrical current between the source and drain electrodes was observed. In a rough estimation based on 3D network model,[29] it can be inferred that in case the percolation path for Co particles has been formed, the volume fraction of Co in the system consisting of Co and Li_2O is at least 0.3.[29] This value is already larger than the volume ratio of Co to Li_2O as a result of lithiation, indicating that the possibility of forming percolation paths consisting of solely Co particles is small. This is consistent with our picture in which Co particles are dispersed in Li_2O matrix.

Additionally, the formation of the Co/Li_2O bulk heterojunction interface induces a high denisty of carrier trapping centers. It is known that the presence of the carrier trapping centers leads to significant decrease in the carrier mobility.[25] According to the thermal carrier trapping and release model in disordered nanostructures,[25] consistent with the thermally activated transport mechanism in Figure 3b, the carrier mobility, μ, depends on the density of the localized states as given in the relation, $\mu = \mu_0(N_f/(N_f + N_t)$, where N_f and N_t represent the density of free carriers and localized states, respectively. Indeed, a large hysteresis, a signature of the presence of the localized states, was observed after a number of cycles (see the Supporting Information Figure S3b). For a pristine device without electrochemical reactions, no hysteresis was observed in which the magnitude of the current was independent of the sweep direction of the source−drain voltage. However, for the device exposed to two cycles of lithiation and delithiation, current−voltage measurements showed large hysteresis for the film. This hysteresis indicates that a high density of charge carrier traps was produced because structural defects were introduced during the fomation of the Co and Li_2O bulk heterojunction interface. This is consistent with the result from Wang *et al.*[30] in which X-ray diffraction peaks for Co_3O_4 and Co as results of lithiation and delithiation processes were not observed because both the degree of crystallinity and the size of nanoparticles decreased, increasing the degree of structural defects, as a source of trapping centers.

The introduction of structural trap sites can be inferred from a drastic morphology change in Co_3O_4 NPs, as seen in the SEM images in Figure S4. According to Poizot *et al.*,[11] reversible decomposition of Li_2O to form the Co_3O_4 phase is predicted in the following charging (delithiation) process after the first lithiation. However, further decrease in the electronic conductance from our experiments implies that the morphological change after the first lithiation is dramatic even if the compositional change is assumed to be reversible. These results are consistent with the large initial irreversible capacity loss observed in Figure 2 and will be discussed in relation to the formation of the SEI layer.

In contrast to the thick film, a monolayer Co_3O_4 film showed a rapid conductance drop from 10^{-10} to 10^{-13} S after the first lithiation up to V_{oc} = 0.05 V. After lithiation, a significant conductance decrease in a monolayer thick Co_3O_4 NPs (Figure S3a) is in sharp contrast to the significant current increase seen for the

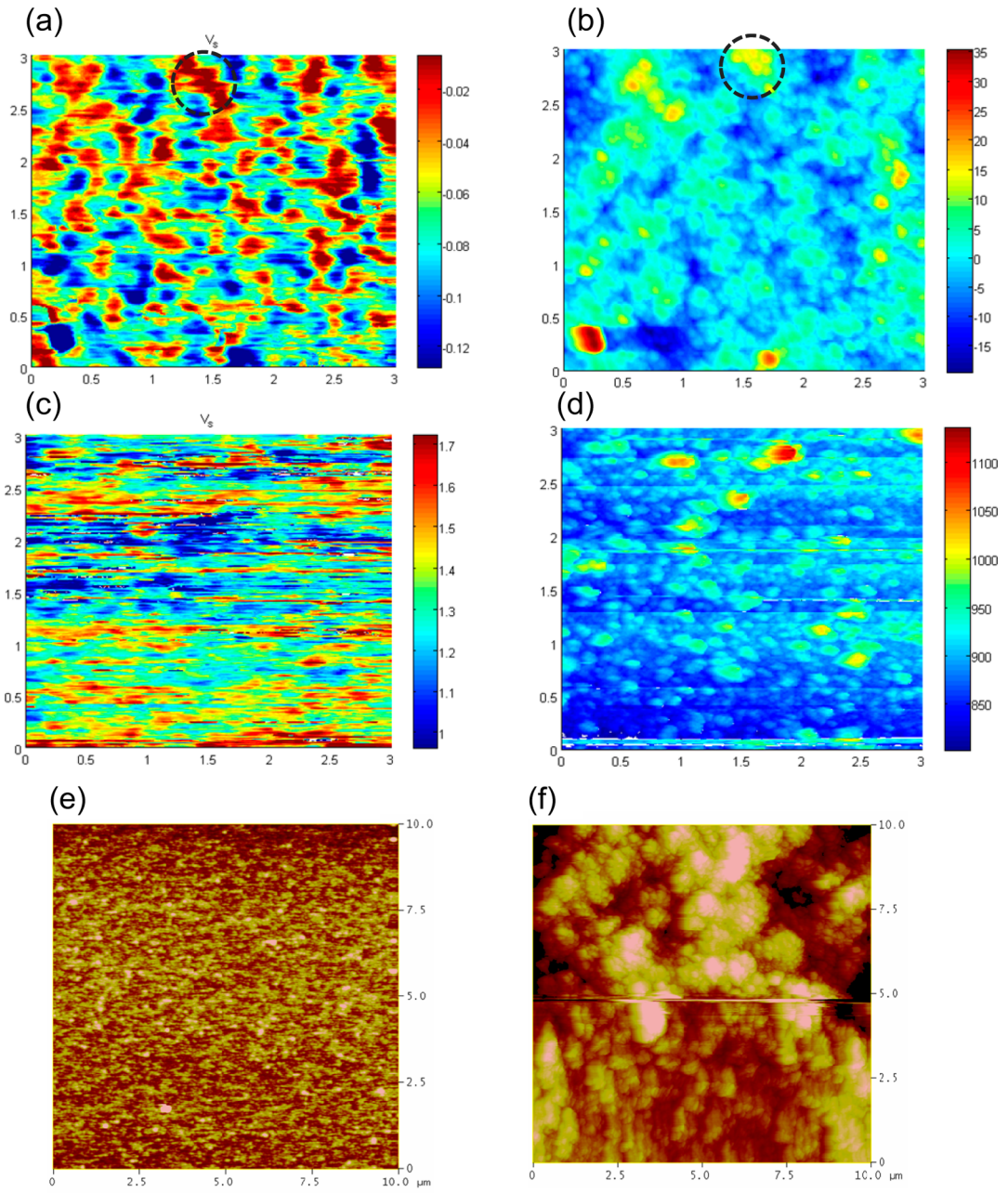

Figure 4. Surface potential (a,c) and height images (b,d) acquired from EFM and tapping-mode AFM for a thick Co_3O_4 NP film, respectively. The surface potential (a) and height (b) images were obtained before battery cycles. The surface potential (c) and height images (d) were measured after the first lithiation. (e) AFM images before battery cycles and (f) after several cycles for a thin (several layers) Co_3O_4 NP film.

thick Co_3O_4 NP film in Figure 3d. This result is insightful because any change in the conductance of a monolayer film is reflective of any interfacial electrochemical reactions that result from lithiation. The significant drop in the conductance of the monolayer film is suggested to arise from a dramatic increase in the electrical contact resistance between NPs and/or loss in the conducting path due to structural defects produced during electrochemical reactions. Electrically "poor" contacts between NPs are expected from the surface morphology in Figure S4, to be discussed below.

Significant electronic and structural changes for NPs at the front in direct contact with electrolyte was evidenced by EFM and AFM in Figure 4. EFM potential and AFM height images for a thick Co_3O_4 film in Figure 4a,b show that the top of NP mounds (dashed region) is more positively charged than that in the valley (blue colored region). After lithiation, the polarity between the top and valley of the film for pristine and lithiated samples was reversed. For the lithiated sample in Figure 4c,d, the image of the surface potential became featureless. The images indicate that, during lithiation, the surface was electrochemically modified

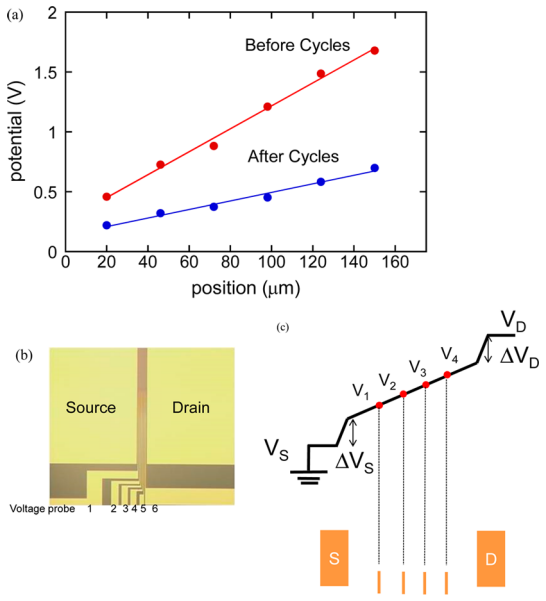

Figure 5. Potential measurements along the Co_3O_4 channel region between the source and drain electrodes. (a) Plot of potential as a function of position from the source electrode. A drain voltage of 2 V was applied during potential measurements. (b) Optical micrograph of a device with multiple voltage probes between the source and drain electrodes. (c) Schematic diagram representing the voltage drops at the source (ΔV_S) and the drain electrodes (ΔV_D).

accompanied by the formation of Co and Li_2O. Particulaly, the electrostatic change on the top enables us to infer that, for the monolayer NP film in Figure 2a, the electronic properties were severely altered. Additionally, after a number of cycles, the roughness dramatically increased as a result of lithium intercalation as seen in the increase in the rms roughness from 3.9 to 113 nm in Figure 4e,f. These observations suggest that electrical and structural degradation at the front of a Co_3O_4 film are immediate and significant during battery discharging, supporting a higher initial capacity loss in a monolayer sample than that in a thick film, as seen in Figure 2a,b.

To address the origin of the initial irreversible capacity loss, increase in the electrical contact resistance between the current collector and Co_3O_4 NP film should be explored. A thick Co_3O_4 NP film was deposited between source and drain electrodes using EPD, and the potential profiles along the channel were acquired using prepatterned multiple voltage probes between the metal electrodes as seen in Figure 5a. Before electrochemical reactions in a liqud electrolyte, the potentials were measured as a function of position in Figure 5b. Voltage drops at the source and drain electrodes were calculated from a linear fitting of the potentials measured in the channel region *versus* position, as shown in Figure 5c. In a pristine device, the voltage drops at the source (ΔV_S) and drain electrodes (ΔV_D) were 0.26 and 0.16 V, respectively, indicating that the electrical contact resistance which can be a bottleneck for electronic transport is not negligible. A higher voltage drop at the source electrode in comparison with that at the drain electrode is typical for a contact with a high injection barrier.[31,32]

After the first lithiation/delithiation cycle, the potential profile changed remarkably, featuring a far larger voltage drop (1.4 V) at the drain electrode than that (0.14 V) at the source electrode (Figure 5). The nature of carrier injection from the current collector into Co_3O_4 NPs was investigated from the temperature-dependent voltage drop measurements at the metal electrodes in Figure S5 (see the Supporting Information). At a lower temperature (240 K), a higher voltage drop was observed, indicating that carriers are transferred into Co_3O_4 by thermionic emission in which a certain thermal energy is required to overcome the barrier set by the energy of the carriers. The large contact resistance associated with thermionic emission at the drain electrode has reproducibly been observed in devices with highly disordered polycrystalline materials near metal electrodes, suggesting that Co_3O_4 NPs are highly damaged during lithiation/delithiation near metal electrodes (*i.e.*, current collectors).[32,33] It is noted that the contact resistance increased by a factor of 3 while the channel resistance decreased by a factor of 10. Further, we suspect that a larger discharge capactity than the charge capacity in the first few cycles (Figure 2a,b) is partly due to more efficient carrier injection (discharging) into Co_3O_4 NPs than carrier extraction (charging), as demonstrated in the higher contact resistance in the drain electrode after the first cycle.

As possible origins of the irreversible capacity loss, the formation of the SEI layer and side reactions associated with liquid electrolyte have been investigated.[10,34−36] Indeed, change in the surface potential from EFM in Figure 4 can be attributed to the formation of the SEI layer, consuming carriers, and/or Li ions. In monolayer thick electrochemical transistors, the contribution of the SEI layers in determining the electrochemical properties of the device is far significant in comparison with thick films. Indeed, the sloping regions in the discharging curves (Figure 2) are remarkably different, implying that intercalation of Li through SEI is dominant. Importantly, the irreversible capacity loss was more significant in the monolayer thick transistor than in the thick film transistor. It is known that the formation of the SEI layer is immediate after the first lithiation.[37] SEI layers are electronically resistive, while the ionic conductivity is substantial, allowing Li ions to diffuse through it.[37] After the first lithiation, therefore, monolayer Co_3O_4 films are covered with electronically resistive SEI layers, leading to the current level below tens of picoampere.

In addition to the formation of the SEI layer, the formation of electronic trap states, as confirmed by huge hysteresis in Figure S3 (Supporting Information), can contribute to the irreversible capacity loss by

reducing the subsequent electrochemical reactions after the first lithiation process in which a number of trap centers are created. The abrupt morphology change in the conversion reaction can be inferred through comparison with alloying and dealloying process for Sn or Al in which the change in the conductance does not occur until tens of cycles. [Data not shown] For the samples, no significant hysteresis was observed after tens of cycles.

From the electronic conduction change in Figure 3, during lithiation and delithiation, incomplete Li_2O decomposition during oxidation of Co particles can be another source for capacity loss. Indeed, the formation of Li_2O is thermodynamically favorable during discharging, while extraction of Li from Li_2O is not feasible, explaining irreversible change in the electrical conductance in Figure 3d. According to Poizot *et al.*,[11] based on TEM results, it was claimed that the formation and decomposition of Li_2O is a reversible process, in contradiction to our results. In a large area unobservable by TEM, however, the electronic conduction measurements of Figure 3 suggest a possibility that remnant Li_2O, independent of charging/discharging processes, can disturb electronic conduction pathways in the Co_3O_4 NP channel. According to Kang *et al.*,[15] addition of Co into Li_2O led to far larger oxidation and reduction peaks from CV experiments in comparison to those without Co, implying that reversible formation and decomposition of Li_2O can be facilitated or suppressed depending on local composition during charging/discharging. Indeed, it was claimed that the reversible formation and decomposition of Li_2O depends on the size and catalytic effect of the transition metal.[11,16]

Further, incomplete Li_2O decomposition at the interface between electrolyte and Co_3O_4 can be critical in causing irreversible capacity loss, as demonstrated by the capacity loss difference between monolayer and thick Co_3O_4 electrochemical transistors in Figure 2. As supported by the previous studies,[15,30] Co is not readily available due to electrochemical reactions with electrolyte, hampering decomposition of Li_2O during further lithiation and delithiation. Indeed, due to formation of electrically resistive Li_2O islands at the interface, the electronic conductivity in a monolayer transistor showed a dramatic decrease in Figure S3a (Supporting Information).

Additionally, decrease in the number of electronic carriers due to increase in the contact resistance at the current collector/electrode can increase the irreversible capacity loss. The increase in the contact resistance as demonstrated in Figure 5 arises from poor physical contact due to structural defects at the current collector/electrode interface and (or) energy barrier at the metal/semiconductor contact.[25,38] Change in the energy barrier for carriers as a result of the lithiation/delithiation process cannot be confirmed in our experiments. However, formation of structural defects can be

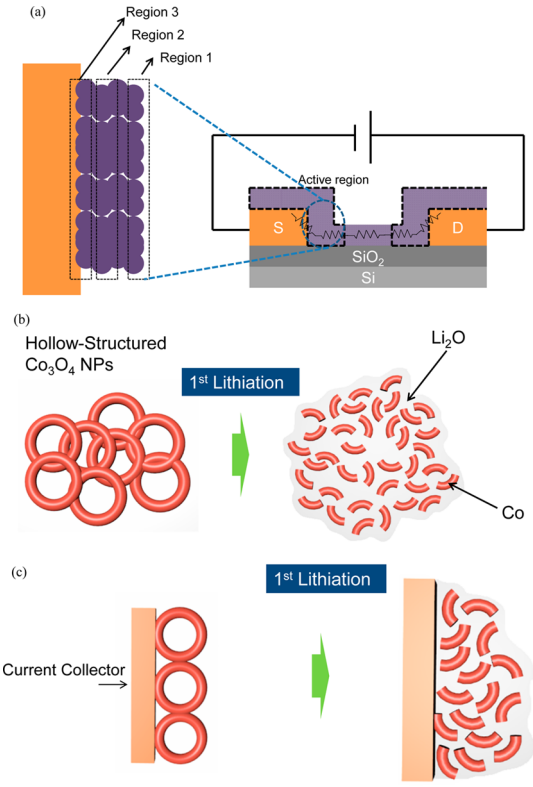

Figure 6. Schematic diagrams for (a) the arrangement of a Co_3O_4 two contact device, structural change (b) in the channel and (c) near the metal contacts (current collector) between the source and drain electrodes after lithiation of Co_3O_4 NPs.

inferred based on the SEM image in the Supporting Information and the abrupt conductivity change after the first lithiaiton in Figure 3d. It is noted that the irreversible capacity loss after the first lithiation for EPD-treated Co_3O_4 NP films was similar independent of the presence of the conductive additives. However, for drop-cast films, the presence of the conductive additives was critical in causing irreversible capacity loss. In other words, without conductive additives, the capacity loss in drop-cast films was far larger than that in EPD-treated films. This indicates that for drop-cast films, less dense than EPD-treated films,[13] the role of conductive additives is critical in sustaining the conduction path after the first discharge because change in the film morphology after the first discharge would be more dramatic than for EPD-treated films.

To summarize, the origin of the irreversible capacity loss can be understood from two different perspectives. One is the production of the structures in which carriers or Li ions are consumed, including formation of carrier trapping centers. The other is electronic and structural change in electrode materials at the interface (SEI layer) and bulk, resulting from irreversible electrochemical reactions, which is critical as a universal source of capacity loss. A thick Co_3O_4 NP film can be divided into three distinct regions as displayed in Figure 6. In "Region 1", electrical and structural

degradation, confirmed by a significant conductivity decrease coupled with EFM and AFM results, occurs during lithiation/delithiation. As observed in monolayer transistors, sloping regions in the charging/discharging curves were different from thick Co_3O_4 layers partly due to the formation of the SEI layer on the surface of the Co_3O_4 film in Figure 2. In "Region 2", the electronic and structural modifications in Co_3O_4 NPs are not as severe as those at the front in direct contact with liquid electrolyte. Conversion reactions producing metallic Co nanoclusters increased the electrical conductivity in Co_3O_4 films in the first lithiation process. As noted above, however, the conductance increase was far lower than that caused by the formation of the Co metallic phase. Therefore, it is inferred that Co nanoclusters are surrounded by a more electrically resistive phase, Li_2O, as shown in Figure 6b. In subsequent lithation and delithiation, conductivity decreased dramatically, suggesting that the morphological change, accompanied by the formation and decomposition of the electrically resistive Li_2O phase, is not favorable for efficient electronic transport. The increase in the contact resistance between the current collector and Co_3O_4 NPs after the first lithiation step can be attributed to physically poor contacts induced by the formation of Li_2O at the interface (Figure 6c). This is evidenced by large voltage drops both at the source and drain contacts. Particularly, the increase in electrical traps at the contact between the current collector and Co_3O_4 NPs can increase the voltage drop at the drain electrode. We believe that the increase in the contact resistance between the current collector and NPs in "Region 3" can contribute to the irreversible capacity loss in the initial charging/discharging processes, causing a bottleneck that hampers reversible electrochemical reactions.

CONCLUSIONS

Here, using additive-free nanostructured electrodes in combination with a two-contact electrochemical transistor probe, we demonstrated feasible capacity loss mechanisms which can be applied to most of the electrode materials incorporated in Li-ion batteries during initial lithiation/delithiation process. The use of EPD-treated NP films eliminates complications arising from any additives such as conductive agents and polymer binders. Change in the morphology of materials buried, which cannot be investigated with conventional microscopic techniques, can be addressed through change in the electronic conduction as results of electrochemical reactions. It was found that the structural arrangement after the first lithiation is unfavorable for electronic transport, enabling us to infer that the morphology of the Co_3O_4 NP films changes in the way that Li_2O surrounds Co (lithiation) or Co_3O_4 (delithiation) in a millimeter-sized area after the first lithiation process. The irreversible composition and decomposition of Li_2O during lithiation and delithiation are due to a locally deficient amount of Co. Particularly, Li_2O islands at the surface of Co_3O_4 NP film remained independent of lithiation/delithiation processes, supported by more significant initial capacity loss in a monolayer Co_3O_4 film in comparison to a thick Co_3O_4 film.

Importantly, this system can be utilized as a platform for electrical measurements and (or) microscopic/spectroscopic tools to map out the electronic and structural changes, during lithiation and delithiation, of the entire region including the current collector/electrode interface as well as the bulk electrode. This electrochemical transistor can be complementary to an impedance spectroscopy method, a conventional technique to probe electronic properties of a series of interfaces and bulk depending on the response to particular frequency ranges, in assigning electrical signals from impedance measurements to the relevant interfaces. Particularly, structural characterization using tools such as TEM is limited in the ability to discern large-area morphological changes due to the confined nanosized area of observation. With the system introduced here, a large area from the electrolyte/SEI interface through the current collector/electrode interface can be systemically explored.

MATERIALS AND METHODS

The Co_3O_4 NPs were prepared from cobalt metal NPs. The starting cobalt NP synthesis follows standard procedures.[39] A N_2-flushed three-neck flask was filled with trioctylphosphine oxide (0.1 g) and 0.09 g of oleic acid dissolved in 12 mL of 1,2-dichlorobenzene. When the temperature of the solution reached 180 °C, 0.52 g of $Co_2(CO)_8$ dissolved in 4 mL of 1,2-dichlorobenzene was quickly injected. After the reaction progressed for 5 min, the reaction solution was quenched in a water bath. The cobalt NPs were purified by adding ethanol and centrifuged. The supernatant was removed, and the NPs were redispersed in hexane. This precipitation/redispersion process was performed twice overall.

To assemble Co_3O_4 NPs into films ranging in thickness from a monolayer to multilayers, blade-coating (see the Supporting Information Figure S1) and electrophoretic deposition methods were used. To form thick films (~400 nm), EPD was used as shown in Figure 1a: a strong electric field (~1500 V/cm) was applied between two metal plates to drive Co NPs in solvent (hexane) into a two-contact device placed on a metal plate. Monolayer thick Co_3O_4 NP films were fabricated by blade-coating as shown in Figure S1: a Co solution in hexane at a concentration of 5 mg/mL was dropped onto a substrate placed on a hot plate at a temperature of 60 °C. Then, a glass blade at a constant height from the substrate was scanned at a constant speed of 0.5 mm/s. The Co NP samples prepared using EPD or blade-coating were transferred to a furnace for oxidation. The oxidation was carried out at 200 °C for 2 h in air to convert the Co to Co_3O_4 and remove remaining organic surfactant ligands.[40]

Conflict of Interest: The authors declare no competing financial interest.

Acknowledgment. This work (B.P.) was supported by the 2014 Hongik University Faculty Research Support Fund. E.R. acknowledges the support of the Georgia Institute of Technology. D.-H.K. and H.K. were supported by the Pioneer Research Center Program through the National Research Foundation of Korea funded by the Ministry of Science, ICT & Future Planning (2013M3C1A3065040).

Supporting Information Available: Scanning electrom microscopy images of Co_3O_4 NPs and charge transport and injection data for Co_3O_4 transistors are included. This material is available free of charge *via* the Internet at http://pubs.acs.org.

REFERENCES AND NOTES

1. Wang, Y.; Takahashi, K.; Lee, K.; Cao, G. Z. Nanostructured Vanadium Oxide Electrodes for Enhanced Lithium-Ion Intercalation. *Adv. Funct. Mater.* **2006**, *16*, 1133–1144.
2. Wang, Z. Y.; Zhou, L.; Lou, X. W. Metal Oxide Hollow Nanostructures for Lithium-Ion Batteries. *Adv. Mater.* **2012**, *24*, 1903–1911.
3. Song, H. K.; Lee, K. T.; Kim, M. G.; Nazar, L. F.; Cho, J. Recent Progress in Nanostructured Cathode Materials for Lithium Secondary Batteries. *Adv. Funct. Mater.* **2010**, *20*, 3818–3834.
4. Chan, C. K.; Peng, H. L.; Twesten, R. D.; Jarausch, K.; Zhang, X. F.; Cui, Y. Fast, Completely Reversible Li Insertion in Vanadium Pentoxide Nanoribbons. *Nano Lett.* **2007**, *7*, 490–495.
5. Li, N. C.; Martin, C. R.; Scrosati, B. Nanomaterial-Based Li-Ion Battery Electrodes. *J. Power Sources* **2001**, 240–243.
6. Sides, C. R.; Li, N. C.; Patrissi, C. J.; Scrosati, B.; Martin, C. R. Nanoscale Materials for Lithium-Ion Batteries. *MRS Bull.* **2002**, *27*, 604–607.
7. Bazito, F. F. C.; Torresi, R. M. Cathodes for Lithium Ion Batteries: The Benefits of Using Nanostructured Materials. *J. Braz. Chem. Soc.* **2006**, *17*, 627–642.
8. Arico, A. S.; Bruce, P.; Scrosati, B.; Tarascon, J. M.; Van Schalkwijk, W. Nanostructured Materials for Advanced Energy Conversion and Storage Devices. *Nat. Mater.* **2005**, *4*, 366–377.
9. Binotto, G.; Larcher, D.; Prakash, A. S.; Urbina, R. H.; Hegde, M. S.; Tarascon, J. M. Synthesis, Characterization, and Li-Electrochemical Performance of Highly Porous Co_3O_4 Powders. *Chem. Mater.* **2007**, *19*, 3032–3040.
10. Tarascon, J. M.; Armand, M. Issues and Challenges Facing Rechargeable Lithium Batteries. *Nature* **2001**, *414*, 359–367.
11. Poizot, P.; Laruelle, S.; Grugeon, S.; Dupont, L.; Tarascon, J. M. Nano-sized Transition-Metal Oxides as Negative-Electrode Materials for Lithium-Ion Batteries. *Nature* **2000**, *407*, 496–499.
12. Thorpe, R.; Rangan, S.; Sina, M.; Cosandey, F.; Bartynski, R. A. Conversion Reaction of CoO Polycrystalline Thin Films Exposed to Atomic Lithium. *J. Phys. Chem. C* **2013**, *117*, 14518–14525.
13. Ha, D. H.; Islam, M. A.; Robinson, R. D. Binder-Free and Carbon-Free Nanoparticle Batteries: A Method for Nanoparticle Electrodes without Polymeric Binders or Carbon Black. *Nano Lett.* **2012**, *12*, 5122–5130.
14. Liu, Y.; Mi, C. H.; Su, L. H.; Zhang, X. G. Hydrothermal Synthesis of Co_3O_4 Microspheres as Anode Material for Lithium-Ion Batteries. *Electrochim. Acta* **2008**, *53*, 2507–2513.
15. Kang, Y. M.; Kim, K. T.; Kim, J. H.; Kim, H. S.; Lee, P. S.; Lee, J. Y.; Liu, H. K.; Dou, S. X. Electrochemical Properties of Co_3O_4, Ni−Co_3O_4 Mixture and Ni−Co_3O_4 Composite as Anode Materials for Li Ion Secondary Batteries. *J. Power Sources* **2004**, *133*, 252–259.
16. Kang, Y. M.; Song, M. S.; Kim, J. H.; Kim, H. S.; Park, M. S.; Lee, J. Y.; Liu, H. K.; Dou, S. X. A Study on the Charge−Discharge Mechanism of Co_3O_4 as An Anode for the Li Ion Secondary Battery. *Electrochim. Acta* **2005**, *50*, 3667–3673.
17. Nelson, G. J.; Cassenti, B. N.; Peracchio, A. A.; Chiu, W. K. S. Microstructural Effects on Electronic Charge Transfer in Li-Ion Battery Cathodes. *J. Electrochem. Soc.* **2012**, *159*, A598–A603.
18. Choi, N. S.; Chen, Z. H.; Freunberger, S. A.; Ji, X. L.; Sun, Y. K.; Amine, K.; Yushin, G.; Nazar, L. F.; Cho, J.; Bruce, P. G. Challenges Facing Lithium Batteries and Electrical Double-Layer Capacitors. *Angew. Chem., Int. Ed.* **2012**, *51*, 9994–10024.
19. Liu, X. H.; Liu, Y.; Kushima, A.; Zhang, S. L.; Zhu, T.; Li, J.; Huang, J. Y. *In Situ* TEM Experiments of Electrochemical Lithiation and Delithiation of Individual Nanostructures. *Adv. Energy Mater.* **2012**, *2*, 722–741.
20. Van der Ven, A.; Bhattacharya, J.; Belak, A. A. Understanding Li Diffusion in Li-Intercalation Compounds. *Acc. Chem. Res.* **2013**, *46*, 1216–1225.
21. Kalinin, S.; Balke, N.; Jesse, S.; Tselev, A.; Kumar, A.; Arruda, T. M.; Guo, S. L.; Proksch, R. Li-Ion Dynamics and Reactivity on the Nanoscale. *Mater. Today* **2011**, *14*, 548–558.
22. Zheng, J. C. Recent Advances on Thermoelectric Materials. *Front. Phys. China* **2008**, *3*, 269–279.
23. Du, N.; Zhang, H.; Chen, B.; Wu, J. B.; Ma, X. Y.; Liu, Z. H.; Zhang, Y. Q.; Yang, D.; Huang, X. H.; Tu, J. P. Porous Co_3O_4 Nanotubes Derived from $Co_4(CO)_{12}$ Clusters on Carbon Nanotube Templates: A Highly Efficient Material for Li-Battery Applications. *Adv. Mater.* **2007**, *19*, 4505–4509.
24. Li, W. Y.; Xu, L. N.; Chen, J. Co_3O_4 Nanomaterials in Lithium-Ion Batteries and Gas Sensors. *Adv. Funct. Mater.* **2005**, *15*, 851–857.
25. Baranovski, S. *Charge Transport in Disordered Solids with Applications in Electronics*; John Wiley & Sons: Chichester, UK, 2006.
26. Patil, V.; Joshi, P.; Chougule, M.; Sen, S. Synthesis and Characterization of Co_3O_4 Thin Film. *Soft Nanosci. Lett.* **2012**, *2*, 1–7.
27. Pralong, V.; Leriche, J. B.; Beaudoin, B.; Naudin, E.; Morcrette, M.; Tarascon, J. M. Electrochemical Study of Nanometer Co_3O_4, CO, $CoSb_3$ and Sb Thin Films toward Lithium. *Solid State Ionics* **2004**, *166*, 295–305.
28. Consiglio, R.; Baker, D. R.; Paul, G.; Stanley, H. E. Continuum Percolation Thresholds for Mixtures of Spheres of Different Sizes. *Physica A* **2003**, *319*, 49–55.
29. Kirkpatrick, S. Percolation and Conduction. *Rev. Mod. Phys.* **1973**, *45*, 574–588.
30. Wang, G. X.; Chen, Y.; Konstantinov, K.; Yao, J.; Ahn, J. H.; Liu, H. K.; Dou, S. X. Nanosize Cobalt Oxides as Anode Materials for Lithium-Ion Batteries. *J. Alloys Compd.* **2002**, *340*, L5–L10.
31. Hamadani, B. H.; Corley, D. A.; Ciszek, J. W.; Tour, J. M.; Natelson, D. Controlling Charge Injection in Organic Field-Effect Transistors Using Self-Assembled Monolayers. *Nano Lett.* **2006**, *6*, 1303–1306.
32. Chen, Z. H.; Appenzeller, J.; Knoch, J.; Lin, Y. M.; Avouris, P. The Role of Metal-Nanotube Contact in the Performance of Carbon Nanotube Field-Effect Transistors. *Nano Lett.* **2005**, *5*, 1497–1502.
33. Li, T.; Ruden, P. P.; Campbell, I. H.; Smith, D. L. Investigation of Bottom-Contact Organic Field Effect Transistors by Two-Dimensional Device Modeling. *J. Appl. Phys.* **2003**, *93*, 4017–4022.
34. Goodenough, J. B.; Kim, Y. Challenges for Rechargeable Li Batteries. *Chem. Mater.* **2010**, *22*, 587–603.
35. Zhang, S. S.; Xu, K.; Jow, T. R. Formation of Solid Electrolyte Interface in Lithium Nickel Mixed Oxide Electrodes during the First Cycling. *Electrochem. Solid-State Lett.* **2002**, *5*, A92–A94.
36. Gowda, S. R.; Pushparaj, V.; Herle, S.; Girishkumar, G.; Gordon, J. G.; Gullapalli, H.; Zhan, X. B.; Ajayan, P. M.; Reddy, A. L. M. Three-Dimensionally Engineered Porous Silicon Electrodes for Li Ion Batteries. *Nano Lett.* **2012**, *12*, 6060–6065.
37. Zhang, S. S.; Xu, K.; Jow, T. R. EIS Study on the Formation of Solid Electrolyte. *Electrochim. Acta* **2006**, *51*, 1636–1640.
38. Scott, J. C. Metal−Organic Interface and Charge Injection in Organic Electronic Devices. *J. Vac. Sci. Technol., A* **2003**, *21*, 521–531.

39. Puntes, V. F.; Krishnan, K. M.; Alivisatos, A. P. Colloidal Nanocrystal Shape and Size Control: The Case of Cobalt. *Science* **2001**, *291*, 2115–2117.
40. Ha, D. H.; Moreau, L. M.; Honrao, S.; Hennig, R. G.; Robinson, R. D. The Oxidation of Cobalt Nanoparticles into Kirkendall-Hollowed CoO and Co_3O_4: The Diffusion Mechanisms and Atomic Structural Transformations. *J. Phys. Chem. C* **2013**, *117*, 14303–14312.